Author's Accepted Manuscript

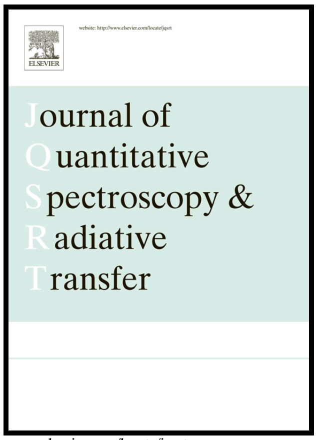

www.elsevier.com/locate/jqsrt

Modeling uncertainties in estimation of canopy LAI from hyperspectral remote sensing data–a Bayesian approach

Petri Varvia, Miina Rautiainen, Aku Seppänen

PII: S0022-4073(16)30759-2
DOI: http://dx.doi.org/10.1016/j.jqsrt.2017.01.029
Reference: JQSRT5576

To appear in: *Journal of Quantitative Spectroscopy and Radiative Transfer*

Received date: 11 November 2016
Revised date: 23 January 2017
Accepted date: 23 January 2017

Modeling uncertainties in estimation of canopy LAI from hyperspectral remote sensing data – a Bayesian approach

Petri Varvia[a], Miina Rautiainen[b,c], Aku Seppänen[a]

[a]Department of Applied Physics, University of Eastern Finland
[b]Department of Built Environment, School of Engineering, Aalto University
[c]Department of Electronics and Nanoengineering, School of Electrical Engineering, Aalto University

Abstract

Hyperspectral remote sensing data carry information on the leaf area index (LAI) of forests, and thus in principle, LAI can be estimated based on the data by inverting a forest reflectance model. However, LAI is usually not the only unknown in a reflectance model; especially, the leaf spectral albedo and understory reflectance are also not known. If the uncertainties of these parameters are not accounted for, the inversion of a forest reflectance model can lead to biased estimates for LAI. In this paper, we study the effects of reflectance model uncertainties on LAI estimates, and further, investigate whether the LAI estimates could recover from these uncertainties with the aid of Bayesian inference. In the proposed approach, the unknown leaf albedo and understory reflectance are estimated simultaneously with LAI from hyperspectral remote sensing data. The feasibility of the approach is tested with numerical simulation studies. The results show that in the presence of unknown parameters, the Bayesian LAI estimates which account for the model uncertainties outperform the conventional estimates that are based on biased model parameters. Moreover, the results demonstrate that the Bayesian inference can also provide feasible measures for the uncertainty of the estimated LAI.

Keywords: leaf area index, spectral invariants, photon recollision probability, reflectance model, uncertainty quantification

1. Introduction

New satellite missions with enhanced spectral resolution (e.g. Sentinel-2, EnMAP) will soon produce extensive coverage of our planet. More efficient methods to handle and interpret environmental information from the large data volumes are urgently needed. So far, applications of hyperspectral remote sensing (also known as imaging spectroscopy) have concentrated on monitoring biochemical properties or functioning of vegetation. However, the added value of these data in estimating also structural variables of forest canopies has not been widely demonstrated. In remote sensing of forest structure, hyperspectral data have mainly been used in the form of narrowband vegetation indices (VI), so that the information content of only a few spectral bands is used to estimate a structural characteristic of the canopy (e.g. [1, 2]). VI based approach also exhibit problems such as significant site-, species- and time specificity (e.g. [3–5]), and do not account for the physical relationship between the forest structure and the observations.

Inversion of physically-based forest reflectance models may offer a solution to using the full information content, and not only selected bands, of hyperspectral data sets. The on-going growth in the availability of hyperspectral remote sensing data sets has indeed increased the use of physically-based modeling [6], and new interpretations for links between canopy structure and detailed spectral features have been proposed (e.g. [7]). However, forest reflectance models usually contain many other unknown variables besides the variable of primary interest; for example, forest background (or understory reflectance) and leaf spectral properties vary significantly even in the same biome. In addition, the effect of forest stuctural parameters, for example leaf area index (LAI), on reflected radiation is usually nonlinear and saturates in very dense canopies. Combined, these two characteristics make the inversion of a forest reflectance model an under-determined and ill-posed problem [8, 9]. The complex nonlinear relationship between the leaf area index and the forest reflectance makes the estimation of LAI sensitive to uncertainties in the other model parameters. Thus, using fixed values in the model inversion will most likely result in unreliable estimates of forest structure. A methodology which makes it possible to take into account the uncertainty in these variables is needed.

Bayesian inference (e.g. [10]) offers a coherent, yet flexible framework for handling model uncertainties in parameter estimation problems. In Bayesian approach, uncertainties are modeled statistically. Also the parameters of primary interest (such as the LAI in the present application) are modeled as random variables, allowing the use of *a priori* information on the parameters. The solution of a Bayesian inference problem is the posterior distribution, i.e., the conditional probability distribution of the unknown parameter given the measurement data. The Bayesian approach has been previously used in remote sensing of forest structural parameters, for example, from multispectral MODIS data by Zhang *et al.* [11]. In this paper, the prior information consisted of constraints for the model unknowns, i.e., the parameters were assumed to be uniformly distributed over feasible intervals. However, more feasible prior information on the statistics of the input parameters of reflectance models is often available. Moreover, studies on the effect of the parameter uncertainties in the LAI estimates and the feasibility of the Bayesian approach to recover from the errors caused by such uncertainties have not yet been reported.

The present work focuses on estimating LAI of forest canopies using hyperspectral data. A set of numerical simulations is carried out to study the effect of unknown reflectance model parameters to conventional LAI estimates which use fixed model parameters. Further, we study whether the LAI estimates could recover from errors caused by unknown reflectance model parameters, when a Bayesian approach is taken. In the Bayesian inference, informative, data-based prior models for the reflectance model parameters are written. In addition to evaluating Bayesian point estimates for LAI, the feasibility of Bayesian uncertainty estimates is investigated; in particular, we study how well the Bayesian credible intervals represent the uncertainty of the estimated LAI.

2. Materials and methods

2.1. Forest reflectance model

In this work, forest spectra (i.e. hyperspectral measurements) are modeled using the PARAS forest reflectance model [12] which is based on the concept of photon recollision probability. The PARAS model has the advantage of containing relatively few independent variables and performing well in boreal forests [12]. The bidirectional reflectance factor (BRF) of a forest, $r(\theta_1, \theta_2, \lambda)$, for a given solar zenith angle θ_1, viewing zenith angle θ_2, and wavelength λ, is modeled as: [12]

$$\begin{aligned} r(\theta_1, \theta_2, \lambda) &= \rho_g(\theta_1, \theta_2, \lambda) t_c(\theta_1) t_c(\theta_2) \\ &+ f(\theta_1, \theta_2, \lambda) i_c(\theta_1) \frac{\omega_L(\lambda) - p\omega_L(\lambda)}{1 - p\omega_L(\lambda)}, \end{aligned} \tag{1}$$

where ρ_g is the BRF of the understory layer, t_c is the tree canopy transmittance, $i_c = 1 - t_c$ the tree canopy interceptance, f the canopy upward scattering phase function and ω_L the leaf single scattering albedo. The photon recollision probability p is used in the model to describe the aggregated structure of forest canopies. It is the probability that a photon, after having survived an interaction with a canopy element, will interact with the canopy again.

The first term in Equation (1) describes the part of radiation that has penetrated the tree layer canopy and reflected upwards through the tree canopy after interacting with the understory layer. The second term models the radiation that has hit the tree canopy and scattered in the viewing angle. Even though the model ignores multiple interactions between the tree and understory layers, it has simulated reflectance factors similar to those obtained from satellite images [12]. If the model were to be used in snow conditions, i.e. with a highly reflecting background, modifications would be needed [13].

In this study, the following assumptions and approximations are made in parameterizing the PARAS model. We assume that LAI is related to the effective leaf area index ($\mathrm{LAI_{eff}}$, commonly measured by e.g. the LAI-2000 Plant Canopy Analyzer) through a species-specific shoot clumping factor β so that $\mathrm{LAI_{eff}} = \beta\mathrm{LAI}$. Factor β, in turn, is related to the shoot silhouette-to-total-area ratio (STAR) as $\beta = 4\mathrm{STAR}$.

The photon recollision probability p is approximated according to [14] as

$$p = 1 - \frac{1 - t_d}{\mathrm{LAI}} = 1 - \frac{\beta(1 - t_d)}{\mathrm{LAI_{eff}}}, \tag{2}$$

where t_d is the diffuse transmittance for the tree canopy layer. The canopy transmittance is modeled using Beer-Lambert's law as

$$t_c(\theta) = \exp\left(-\frac{\beta}{2}\frac{\mathrm{LAI_{eff}}}{\cos\theta}\right), \tag{3}$$

from which the diffuse canopy transmittance t_d in equation (2) is calculated following [13]:

$$t_d = 2\int_0^{\frac{\pi}{2}} t_c(\theta)\cos(\theta)\sin(\theta)\mathrm{d}\theta. \tag{4}$$

The upward scattering phase function $f(\theta_1, \theta_2, \lambda)$ is approximated using the proportion of upward scattered radiation Q as [15]

$$f(\theta_1, \theta_2, \lambda) \approx Q = \frac{1}{2} + \frac{q}{2}\frac{1 - p\omega_L}{1 - pq\omega_L}, \tag{5}$$

where q in is a wavelength independent semi-empirical scattering asymmetry parameter. Parameter q describes the decrease in probability of the photon escaping the canopy with increasing scattering order, in other words, it models how photon escape probability decreases as the photon scatters deeper inside the canopy. Thus q is related to canopy density and increases with LAI (Table 2 in [15]).

2.1.1. Wavelength dependence

Leaf albedo ω_L and understory reflectance ρ_g are wavelength dependent parameters. Thus, in the model, ω_L and ρ_g are vectors of the same length as the satellite-measured data vector. To reduce the number of unknown variables in the inverse problem, we utilize known features of the vegetation spectra: The (green) vegetation spectra have a typical shape which features strong correlations between reflectance parameters corresponding to certain wavelengths and discrete jumps across other wavelength intervals. (For further discussion and references to experimental works on determining the vegetation spectra, see Section 2.2.2). This enables the use of reduced order parametric representations for ω_L and ρ_g. More specifically, we use cubic monotone Hermite splines to represent the spectral variables using 27 manually chosen node points that are illustrated in Figure 1. The cubic monotone Hermite spline is monotone between the node points and thus the curve can change direction only on a node. By placing the node points on the typical peaks and troughs of the vegetation spectrum, with additional control nodes in between, the spline representation can follow the typical shape of the spectrum with sufficient accuracy. Figure 1 also shows an example of how the spline representation follows an original spectrum. Using the spline, the variables ω_L and ρ_g are rewritten as

$$\omega_L = S(\lambda; \tilde{\lambda}, \tilde{\omega}_L), \tag{6}$$

$$\rho_g = S(\lambda; \tilde{\lambda}, \tilde{\rho}_g), \tag{7}$$

where $S(\,\cdot\,)$ is the spline function (piecewise polynomial), $\tilde{\lambda} \in \mathbb{R}^{27}$ is a vector consisting of wavelengths corresponding to the spline nodes, and $\tilde{\omega}_L \in \mathbb{R}^{27}$ and $\tilde{\rho}_g \in \mathbb{R}^{27}$, respectively, are the values of ω_L and ρ_g at the node points $\tilde{\lambda}$. Because $\tilde{\lambda}$ is fixed, the spline approximations (6) and (7) are fully determined by $\tilde{\omega}_L$ and $\tilde{\rho}_g$, respectively. Thus, using the spline approximations, the low-dimensional vectors $\tilde{\omega}_L$ and $\tilde{\rho}_g$ are substituted for full-length ω_L and ρ_g as variables in the reflectance model.

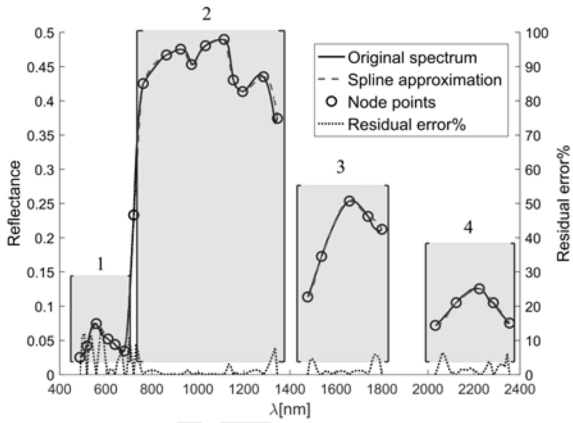

Figure 1: Spline approximation of a vegetation spectrum (synthetic understory reflectance) of 150 spectral bands, the original spectrum is shown with a solid line, the spline approximation with dashed line and the node points of the spline approximation with circles. The relative error between the approximation and the spectrum is shown with a dotted line. The figure also shows the division of the spectrum to correlated parts.

2.2. Bayesian inversion

Let us denote the vector of satellite measured bidirectional reflectances on the $N_\lambda = 150$ spectral bands by $r \in \mathbb{R}^{150}$ and the vector of unknown variables by $x = \begin{bmatrix} \mathrm{LAI}_{\mathrm{eff}} & \tilde{\omega}_L^T & \tilde{\rho}_g^T & \beta \end{bmatrix}^T \in \mathbb{R}^{56}$. In the following, the problem of estimating the unknown model parameters x from the satellite measurements r is formulated as a problem of Bayesian inference. In a Bayesian setting, both the measurements r and the model unknowns x are modeled as random variables.

Let the parameters x have a prior probability density $\pi(x)$, which contains the available information on x before the reflectance measurements have been done. In

Bayesian inference, the prior density is then updated with the information gained from the measurements by using the Bayes theorem

$$\pi(x|r) = \frac{\pi(r|x)\pi(x)}{\pi(r)} \propto \pi(r|x)\pi(x), \quad (8)$$

where $\pi(r|x)$ the likelihood function containing the information from the measurements, and $\pi(x|r)$ is the posterior density for the unknowns x, i.e., the conditional probability density of x given the measurements r. The posterior density $\pi(x|r)$ is the full solution of a Bayesian inverse problem; Section 2.2.3 discusses the exploration of the posterior density with an MCMC method, i.e., finding useful point and spread estimates (such as posterior mean and credibility intervals) for x. The term $\pi(r)$ in Eq. (8) can be thought of as a normalizing constant.

2.2.1. The likelihood function

The likelihood function $\pi(r|x)$ in theorem (8) is derived from the measurement model. Here, we model the measurements r as

$$r = h(x) + e, \quad (9)$$

where $h(x)$ is the PARAS model (1), including the approximations (2), (5), (6), and (7), and $e \in \mathbb{R}^{150}$ is an additive error term. The error e describes the discrepancy between the PARAS model output and the measured r and contains both the model error and the measurement noise.

In the case of the additive error model (9), the likelihood function $\pi(r|x)$ gets the form

$$\pi(r|x) = \pi_e(r - h(x)), \quad (10)$$

where $\pi_e(\,\cdot\,)$ is the density function of e. Here e is modeled as a multivariate normal distributed random variable with a zero mean and a covariance matrix Γ_e, and hence, the likelihood function is

$$\pi(r|x) \propto \exp\left(-\frac{1}{2}(r - h(x))^T \Gamma_e^{-1}(r - h(x))\right). \quad (11)$$

The error e is modeled as uncorrelated, with standard deviation of 10% of the data r in each band.

2.2.2. The prior density

The prior density $\pi(x)$ is a critical part of the Bayesian approach. In this work, separate prior densities for $\mathrm{LAI_{eff}}$, $\tilde{\omega}_L$, $\tilde{\rho}_g$ and β are constructed. Uniform densities are used as priors for the scalar variables $\mathrm{LAI_{eff}}$ and β. For the spectral variables $\tilde{\omega}_L$ and $\tilde{\rho}_g$, Gaussian approximations are build based on empirical data that have been presented in the literature. The complete prior density $\pi(x)$ is finally formed by combining the variable-specific prior densities under the assumption of mutual statistical independence between $\mathrm{LAI_{eff}}$, $\tilde{\omega}_L$, $\tilde{\rho}_g$ and β.

The effective LAI is by definition non-negative; also exceedingly large values of LAI are absent in a typical forest. As a prior distribution for $\mathrm{LAI_{eff}}$ we use a uniform distribution in the interval $[0, 10]$:

$$\pi(\mathrm{LAI_{eff}}) = \begin{cases} \frac{1}{10}, & 0 \leq \mathrm{LAI_{eff}} \leq 10 \\ 0, & \text{otherwise.} \end{cases} \quad (12)$$

Leaf albedo (ω_L) measurements for the three most common tree species in Finnish boreal forest (Scots pine, Norway spruce, and birch species) were reported by Lukeš *et al.* [16]. In our prior construction, the average of these species-specific albedos is used as the prior expected value for the node-point leaf albedo $\tilde{\omega}_L$, denoted with $\mu_{\tilde{\omega}_L}$. Peltoniemi *et al.* [17] presented reflectance measurements (BRF) of several common understory types. The average of these measurements is used as the prior expected value for node-point understory reflectance $\tilde{\rho}_g$, denoted with $\mu_{\tilde{\rho}_g}$. Note here that the reported $\tilde{\omega}_L$ and $\tilde{\rho}_g$ are averaged only over the tree species, not over the wavelength, and hence $\mu_{\tilde{\omega}_L}$ and $\mu_{\tilde{\rho}_g}$ are vectors consisting of the average leaf albedos and understory reflectances corresponding to 27 wavelenghs $\tilde{\lambda}$. For both $\tilde{\omega}_L$ and $\tilde{\rho}_g$ the prior standard deviation was set to 20% of the expected value. This amount of variance was found to allow adequate range of possible $\tilde{\rho}_g$ and $\tilde{\omega}_L$ values while still constraining the solution space sufficiently. The prior expected value and 95% credible intervals for ω_L and ρ_g are shown in Figure 2. The figure also includes the spectral data [16, 17] used for constructing the corresponding prior densities.

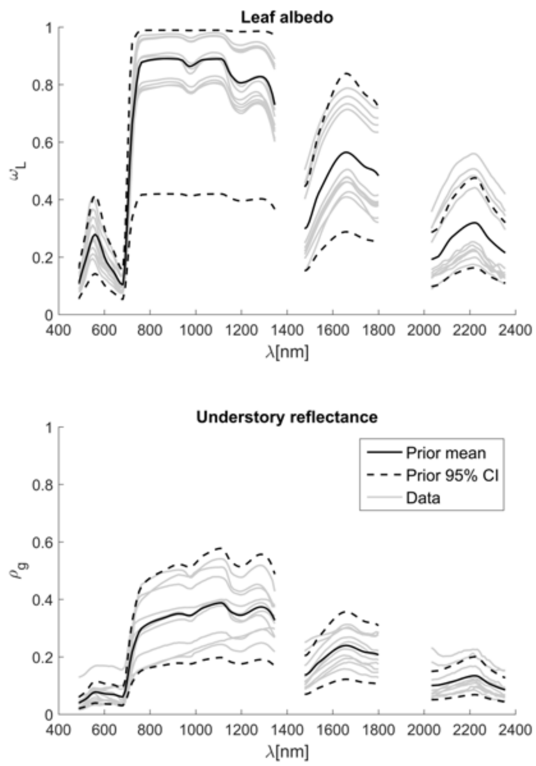

Figure 2: The expected values and 95% credible intervals for the prior densities of ω_L (top) and ρ_g (bottom), and the data used for constructing the priors.

The vegetation spectra have strong spectral correlation structure which is utilized in the prior. The model for the correlation structure of both ω_L and ρ_g is written as follows: First, an uncorrelated Gaussian noise component is written to model the independent variations of the values of ω_L and ρ_g at the node points (i.e. elements of $\tilde{\omega}_L$ and $\tilde{\rho}_g$). Secondly, the measured band is divided into four non-overlapping parts (Figure 1), and the node points within each part are taken to be mutually strongly correlated. Thirdly, the background variation in the spectra is modeled with an additional correlation shared by all the nodes. The four parts in Figure 1 were chosen to reduce the correlation over the red edge between parts 1 & 2, and the water absorption bands between parts 2 & 3 and 3 & 4. This makes the prior fit better to different canopy and understory species compositions.

The associated prior correlation matrix R is thus

$$\begin{aligned} R = {} & \kappa_{\text{ind.}} \underset{27\times27}{I} + \kappa_{\text{part}} R_{\text{part}} + \kappa_{\text{all}} \underset{27\times27}{\mathbf{1}}, \\ & \text{s.t. } \kappa_{\text{ind.}} + \kappa_{\text{part}} + \kappa_{\text{all}} = 1, \end{aligned} \tag{13}$$

where $\kappa_{\text{ind.}}$ is the strength coefficient of uncorrelatedness, κ_{part} is the strength coefficient of correlation within the four band parts shown in Figure 1, κ_{all} is the strength coefficient of background correlation, I is identity matrix, $\mathbf{1}$ is a matrix consisting of ones, sizes of the matrices are denoted under the symbols, and finally

$$R_{\text{part}} = \begin{bmatrix} \underset{6\times6}{\mathbf{1}} & 0 & 0 & 0 & 0 \\ 0 & \underset{1\times1}{I} & 0 & 0 & 0 \\ 0 & 0 & \underset{10\times10}{\mathbf{1}} & 0 & 0 \\ 0 & 0 & 0 & \underset{5\times5}{\mathbf{1}} & 0 \\ 0 & 0 & 0 & 0 & \underset{5\times5}{\mathbf{1}} \end{bmatrix}. \tag{14}$$

In this study we use the values $\kappa_{\text{ind.}} = 0.3$, $\kappa_{\text{part}} = 0.4$, $\kappa_{\text{all}} = 0.3$.

Using the correlation matrix R, the prior covariance matrices for $\tilde{\omega}_L$ and $\tilde{\rho}_g$ are then respectively

$$\Gamma_{\tilde{\omega}_L} = S_{\tilde{\omega}_L} R S_{\tilde{\omega}_L} \quad (15)$$

$$\Gamma_{\tilde{\rho}_g} = S_{\tilde{\rho}_g} R S_{\tilde{\rho}_g}, \quad (16)$$

where $S_{\tilde{\omega}_L}$ and $S_{\tilde{\rho}_g}$ are diagonal matrices that contain the prior standard deviations of $\tilde{\omega}_L$ and $\tilde{\rho}_g$ on their main diagonal. With the expected values and the covariance matrices, the Gaussian prior densities for $\tilde{\omega}_L$ and $\tilde{\rho}_g$, constrained to the range [0, 1], are

$$\pi(\tilde{\omega}_L) \propto \begin{cases} \exp\left(-\frac{1}{2}(\tilde{\omega}_L - \mu_{\tilde{\omega}_L})^T \Gamma_{\tilde{\omega}_L}^{-1} (\tilde{\omega}_L - \mu_{\tilde{\omega}_L})\right), & 0 \leq \tilde{\omega}_L \leq 1 \\ 0, & \text{otherwise,} \end{cases} \quad (17)$$

$$\pi(\tilde{\rho}_g) \propto \begin{cases} \exp\left(-\frac{1}{2}(\tilde{\rho}_g - \mu_{\tilde{\rho}_g})^T \Gamma_{\tilde{\rho}_g}^{-1} (\tilde{\rho}_g - \mu_{\tilde{\rho}_g})\right), & 0 \leq \tilde{\rho}_g \leq 1 \\ 0, & \text{otherwise.} \end{cases} \quad (18)$$

Due to the monotonicity of the chosen spline representations (6) and (7), constraining only the node points to the physically possible range [0, 1] is sufficient to keep the spectral variables ω_L and ρ_g in that range everywhere.

The shoot clumping parameter β for the coniferous species varies between 0.4 and 0.6 [18]. For broadleaved species, $\beta = 1$ by definition. Defining β for mixed canopies is problematic. For the sake of practicality it is assumed that there is an effective canopy-wide β that describes the average shoot clumping effect. We take this to be the weighted average of species-specific β's. For β we use a uniform prior on the interval [0.4, 1]

$$\pi(\beta) = \begin{cases} \frac{5}{3}, & 0.4 \leq \beta \leq 1 \\ 0, & \text{otherwise.} \end{cases} \quad (19)$$

It would be possible to model also the correlations between the variables $\mathrm{LAI_{eff}}$, β, $\tilde{\omega}_L$ and $\tilde{\rho}_g$. However, quantified information on these correlations is scarce. Therefore it is approximated that these variables are mutually independent. With this approximation, the resulting prior density for x is

$$\pi(x) = \pi(\mathrm{LAI_{eff}})\pi(\tilde{\omega}_L)\pi(\tilde{\rho}_g)\pi(\beta). \quad (20)$$

2.2.3. *The posterior density and estimates*

Substitution of equations (11) and (20) to the Bayes' theorem (8) gives out the posterior density $\pi(x|r)$. The posterior density is used for computing point and interval estimates for the variables x. In this study, the posterior mean is used as the point estimate for x. As an interval estimate, 95% credible intervals are computed. A 95% credible interval for variable $x_i \in \mathbb{R}$ is an interval $[a, b]$ that satisfies

$$\int_a^b \pi(x_i|r) dx_i = 0.95, \quad (21)$$

where $\pi(x_i|r)$ is the posterior marginal density of the variable x_i. Note that here x_i is a single element of the parameter vector x, such as the effective LAI or leaf albedo on a single band. Equation (21) has no unique solution: in this study the interval is chosen such that the probability mass below and above the interval $[a, b]$ is equal.

Computation of the posterior mean and credible intervals requires integration over the posterior density. This can be accomplished numerically using for example Markov chain Monte Carlo (MCMC) methods (e.g. [19]). In MCMC methods, a random walk is used to draw samples from the underlying distribution and these samples are then used to approximate statistics of the distribution.

As the MCMC method, we use the delayed rejection adaptive Metropolis (DRAM) algorithm [20]. The DRAM algorithm is formulated as follows. Denote a

Gaussian proposal distribution by $q(y; \lambda, C)$, where μ is the expected value and C is the covariance matrix. This distribution is used to generate the next proposed state in the random walk.

1. Initialization: Choose a point $x^{(0)}$ to be the start state of the random walk and choose an initial proposal covariance matrix C.
2. Metropolis step, do for each iteration i:
   (a) Sample a candidate $y^{(i)}$ from the proposal distribution $q(y; x^{(i-1)}, C)$ (the Gaussian proposal distribution is now centered on the previous state $x^{(i-1)}$).
   (b) Calculate acceptance ratio:
   $$\alpha_1 = \frac{\pi(y^{(i)}|r)}{\pi(x^{(i-1)}|r)}.$$
   (c) Accept the new candidate $y^{(i)}$ with probability $\min\{1, \alpha_1\}$. If accepted, set $x^{(i)} = y^{(i)}$.
3. Delayed rejection step, do if the candidate $y^{(i)}$ was rejected:
   (a) Sample a new candidate $\eta^{(i)}$ from the second level proposal distribution $q(\eta; x^{(i-1)}, \gamma C)$, where γ is a scaling factor.
   (b) Calculate
   $$\alpha_{12} = \frac{\pi(\eta^{(i)}|r)}{\pi(y^{(i)}|r)}$$
   (c) Calculate the second level acceptance ratio:
   $$\alpha_2 = \frac{\pi(y^{(i)}|r)q(\eta^{(i)}; y^{(i)}, C)(1-\alpha_{12})}{\pi(x^{(i-1)}|r)q(\eta^{(i)}; x^{(i-1)}, C)(1-\alpha_1)}.$$
   (d) Accept the new candidate $\eta^{(i)}$ with probability $\min\{1, \alpha_2\}$. If accepted, set $x^{(i)} = \eta^{(i)}$, otherwise keep the previous state and set $x^{(i)} = x^{(i-1)}$.
4. Adaptation, do every kth iteration: Compute a new proposal covariance $C = s\mathrm{Cov}(x^{(0)}, \ldots, x^{(i)}) + s\epsilon I$, where $\mathrm{Cov}(x^{(0)}, \ldots, x^{(i)})$ is the sample covariance of the states $x^{(0)}, \ldots, x^{(i)}$, s is a scale parameter, I is an identity matrix and ϵ is a small positive constant. The $s\epsilon I$ term ensures that the new proposal covariance is nonsingular.
5. Run until $i = N + B$, where N is the desired number of samples and B is the length of the burn-in period. Discard the first B states $x^{(0)}, \ldots, x^{(B)}$.

If the steps 3 and 4 are omitted from the above algorithm, it reduces to the standard Metropolis algorithm. The delayed rejection and adaptation steps make the algorithm more efficient than the standard Metropolis and make the method more robust against poorly chosen initial proposal covariance.

In this paper, a total of $N = 600000$ Monte Carlo samples are computed using 12 parallel random walks of 50000 samples each. The length of the burn-in period is chosen to be 5000 samples. In the delayed rejection step of the DRAM algorithm, covariance scaling factor of $\gamma = 0.1$ is used. The adaptation step in DRAM is done after every $k = 200$ iterations, with parameters $\epsilon = 10^{-5}$ and $s = 2.4/\sqrt{56}$.

2.3. Simulation studies

In this study, the effect of unknown reflectance model parameters on the LAI estimates is investigated using synthetic hyperspectral remote sensing (i.e. forest spectral) data. Synthetic data is used for the sake of validation: while the parameters LAI, β, ω_L and ρ_g are laborious to measure on field, the simulation studies allow for comparison of the estimates with the true values. However, care must be taken in analyzing the results, because when using simulated data, not all model inaccuracies are accounted for.

2.3.1. *Simulated stands*

A total of 500 random synthetic boreal forest stands were generated and the forest reflectance was simulated using the PARAS model. The simulated spectra consist of 150 spectral bands emulating the EO-1 Hyperion instrument. First, the dominant tree species (pine, spruce or broadleaved) was chosen with uniform probability. The proportion of the dominant species in the species mixture was sampled uniformly from the interval 50%–100%; the remainder was then randomly divided between the two minority species. The composition of the understory layer was then sampled to roughly emulate the typical species composition of a Finnish boreal forest with the chosen dominant tree species, that is, the understory of broadleaved stands contains mostly grasses and some dwarf shrubs, spruce dominated stands have mosses and bilberry, and pine stands have mosses, lingonberry, heather and lichens. Ranges of the understory components are presented in Table 1.

Table 1: Understory composition of the simulated forest stands.

Species	Pine	Spruce	Broadleaved
Mosses	0 – 50%	40 – 100%	0 – 30%
Bilberry	n/a	0 – 50%	0 – 30%
Lingonberry	0 – 100%	n/a	n/a
Heather	0 – 100%	n/a	n/a
Lichens	0 – 100%	n/a	n/a
Grasses	n/a	n/a	30 – 100%
Soil	0 – 10%	0 – 10%	0 – 10%

The leaf area index was chosen randomly from the uniform distribution $\mathcal{U}(0, 5)$. The leaf albedo ω_L and understory reflectance ρ_g were formed as a linear combination of the experimental values presented in [16] and [17], respectively, according to the sampled species fractions of both the tree layer and the understory. Finally, the shoot clumping factor was sampled based on the tree species combination, with deciduous tree fraction contributing $\beta = 1$, spruce $\beta \sim \mathcal{N}(0.5, 0.05^2)$ and pine $\beta \sim \mathcal{N}(0.6, 0.05^2)$.

After all the input parameters were sampled, the PARAS model was used to simulate the forest reflectance. Gaussian random noise with standard deviation of 10% of the reflectance on each band was added to the modelled reflectance. The variance of this simulated radiometric noise was somewhat higher than in most real instruments to compensate for the lack of systematic errors in the simulated data.

2.3.2. *Maximum likelihood estimates*

The conventional approach to model based estimation of $\mathrm{LAI}_{\mathrm{eff}}$ is to invert the reflectance model corresponding to parameters ω_L, ρ_g and β that are fixed to some *a priori* defined values. We studied the tolerance of such $\mathrm{LAI}_{\mathrm{eff}}$ estimate to misspecification of the parameters ω_L, ρ_g and β. More specifically, we considered conventional maximum likelihood (ML) estimates, obtained by maximizing the likelihood function (11) with respect to $\mathrm{LAI}_{\mathrm{eff}}$.

For each of the 500 study stands, the ML estimate was computed using two choices of parameters ω_L, ρ_g and β: 1) In the first ML estimate, the true parameter values in the corresponding study stand were used. This choice is of course unrealistic, since these parameters are practically always unknown. 2) In the second set of ML estimates, parameters ω_L, ρ_g and β were fixed to their average values over the ensemble of simulated study stand test, i.e., to their population means. The latter estimate can be considered as a solution corresponding to the best realistically available approximation for the parameter values, and is expected to exhibit estimation error that is caused by the misspecification of the parameters.

The one-dimensional optimization problem (maximizing (11) with respect to $\mathrm{LAI_{eff}}$) was solved by brute force to 0.1% accuracy, to ensure that the resulting estimate was the global maximum (due to the nonlinearity, the likelihood has multiple local maxima in some cases). For computational reasons, the range of $\mathrm{LAI_{eff}}$ was constrained to $[0, 10]$.

2.3.3. Bayesian estimates and reference methods

Next, the capability of the Bayesian approach to tackle to problem of unknown model parameters ω_L, ρ_g and β was studied. In the Bayesian inference, $\mathrm{LAI_{eff}}$, ω_L, ρ_g and β were simultaneously estimated from the reflection data, as described in Section 2.2.

The Bayesian estimates were compared with two reference methods: 1) The ML estimates of $\mathrm{LAI_{eff}}$ corresponding to parameters ω_L, ρ_g and β fixed to their population means (see Section 2.3.2), and 2) empirical linear regression with a narrow-band vegetation index (VI).

We compared our new Bayesian approach with a typical empirical vegetation index using two narrow spectral bands. As there are a wide range of spectral indices in applied in hyperspectral remote sensing of vegetation, we selected the simple ratio water index (SRWI) which has recently been reported as the best performing index for estimating $\mathrm{LAI_{eff}}$ in our biome of interest, i.e. the boreal forests [2]. The SRWI is defined as

$$\mathrm{SRWI} = \frac{r_{854}}{r_{1235}}. \qquad (22)$$

To construct the the empirical regression model, first, a separate set of 100 random stands were simulated and the SRWI was calculated for each stand. Ordinary linear regression was then performed between $\mathrm{LAI_{eff}}$ and SRWI in the training set. The regression model was then used to estimate $\mathrm{LAI_{eff}}$ for each of the 500 study stands.

We note that as the empirical VI regression estimate does not rely on a reflectance model, it does not require specifying the model parameters ω_L, ρ_g and β. However, the uncertainty of these parameters does have an implicit effect on the accuracy of the VI regression based $\mathrm{LAI_{eff}}$ estimates: variation of these parameters in the training set obfuscates the correlation between the spectral reflectance data r and $\mathrm{LAI_{eff}}$.

2.3.4. Effect of prior model on Bayesian estimate

We also studied the effect of the prior model on the Bayesian estimate. Hence, in addition to computing the Bayesian estimate corresponding to data based, informative prior models described in Section 2.2, the Bayesian estimate was also computed using uniform priors for all the parameters. The uniform priors simply constrain $\mathrm{LAI_{eff}}$ to the range $[0, 10]$, ω_L and ρ_g to the range $[0, 1]$ and β to $[0.4, 1]$. This estimate corresponds to one introduced by Zhang *et al.* [11].

3. Results and discussion

3.1. Sensitivity of the maximum likelihood estimate to model uncertainties

The results of studing the sensitivity of the ML estimate to model uncertainties is illustrated in Figure 3. When the true values of ω_L, ρ_g and β are used in the reflectance model, the estimated $\mathrm{LAI_{eff}}$ are very close to their true values in almost every study stand (Figure 3, left). Only a few significantly erroneous estimates are present – those estimates probably correspond to large realizations of observation noise. Moreover, the scatter

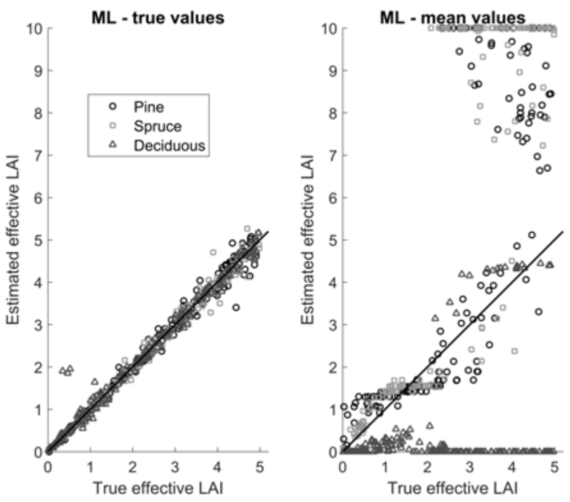

Figure 3: Estimated LAI_{eff} vs. true LAI_{eff} ML estimates corresponding to models with correct values of ω_L, ρ_g and β (left) and their population mean values (right). Pine dominated stands are marked with circles, spruce dominated with squares and deciduous with triangles.

plot shows a slight increase of the estimation error with increasing LAI_{eff}; this is caused by saturation of the forest reflectance: with the increase of LAI, the sensitivity of the reflectance measurements to a change in LAI decreases.

The ML estimates corresponding to the reflectance model with misspecified parameters ω_L, ρ_g and β (Figure 3, right) feature large errors. In particular, ML estimates are zero for several cases where the canopy is dense in reality, and on the other hand, several ML estimates are equal to 10 in cases where the true value of LAI_{eff} is between 2 and 5. In total, 28% of the ML estimates are above the maximum simulated LAI value of 5. We note that accumulation of the ML estimates to values 0 and 10 is a result of bounding these estimates to the interval $[0, 10]$ – without these constraints, many of the estimates would be even more biased.

The root mean square errors (RMSE) and biases of the two ML estimates are shown in Table 2. The comparison of the errors confirms the observation made based on Figure 3: the use of the approximate choices of parameters ω_L, ρ_g and β leads, on average, to large errors in the LAI_{eff} estimates.

The results demonstrate that ML estimates are highly intolerant to misspecification of parameters in the reflectance model. This intolerance is associated with ill-posedness of the inverse problem spanned by the reflectance model – small/moderate errors in the data or model can cause large errors in the estimates. Hence, although only ML estimates were considered in this study, caution should be taken in the interpretation of any model based LAI estimate which does not take into account the uncertainty of the model parameters.

Table 2: RMSE, relative RMSE and bias of effective LAI estimates for the Bayesian posterior mean estimates, the reference empirical VI regression and maximum likelihood estimates.

	RMSE	RMSE%	bias
ML estimate			
- correct model	0.19	7.81	0.0013
- approximate model	3.41	137.78	0.91
Posterior mean			
- informative prior	0.61	24.62	-0.0002
- uniform prior	1.14	45.88	-0.17
VI regression	1.10	44.36	0.11

3.2. Performance of the Bayesian estimates

In this section, we discuss the performance of the Bayesian estimate with informative, data based priors. First, the full Bayesian solutions – including not only the point estimates but also credible intervals of the model unknowns – are illustrated with two example cases: one with low LAI (Section 3.2.1) and one with high LAI (Section 3.2.2). Comparison between the Bayesian estimates and the reference methods is made. Finally, the performance of these estimates is rated based on the statistics of the results corresponding to the set of 500 study stands (Section 3.2.3).

3.2.1. Example 1: low LAI case

The first example stand is a spruce dominated stand with a low leaf area index of $LAI_{eff} = 0.42$. The spectra of ω_L and ρ_g (the 'simulated true values') are depicted in Figure 4. The figure also illustrates the the prior marginal densities of ω_L and ρ_g, and the (fixed) spectra of ω_L and ρ_g used in the ML estimate of LAI_{eff} (see Section 2.3.1) for comparison.

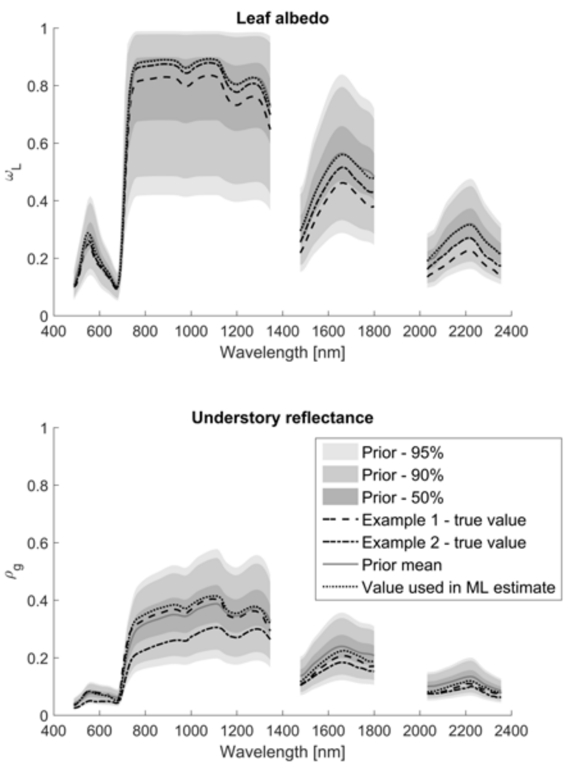

Figure 4: Prior marginal densities and prior expected values of leaf albedo and understory reflectance. The figure also contains the true values of ω_L and ρ_g of the examples 1 and 2, and the assumed values of ω_L and ρ_g used in computing the ML estimates.

The results of Example 1 are illustrated in Figure 5. The top image of Figure 5 represents the Bayesian estimates for the effective LAI corresponding to the informative priors; the posterior mean estimate is marked with a circle, and the 95% credible interval is shaded with gray. The true simulated value of the effective LAI is marked in the figure with a cross.

The Bayesian posterior mean estimate for LAI_{eff} is 0.74, and hence, somewhat overestimates the true value $LAI_{eff}=0.42$. On the other hand, the 95% (posterior) credible interval is $[0.41, 1.07]$, i.e., the true value 0.42 lays inside this interval. It is notable that in this example case the 95% credible interval is significantly narrower than the *a priori* range $[0, 10]$ for LAI_{eff}.

Posterior marginals for the leaf albedo ω_L and understory reflectance ρ_g as function of wavelength are illustrated in the center and bottom of Figure 5 respectively. In the case of low LAI the posterior 95% CI covers the true value of ω_L throughout the range (Figure 5, center). However, the posterior of ω_L is wide, nearly as wide as the prior density in some wavelengths, implying high uncertainty for the estimated values of ω_L. This is an expected outcome: In the case of low LAI, the reflecting surface area of the leaves is small, and the contribution of ω_L to the reflectance measurements is relatively low, i.e., the sensitivity of the measurements to ω_L is low, and consequently, ω_L remains uncertain after the inference from the data.

The posterior density of ρ_g (Figure 5, bottom), on the other hand, is rather narrow. This is again an expected result: In the case of low LAI, the understory has a large effect on the measured reflectance, and in contrary to ω_L, the measurements are sensitive to ρ_g.

The ML estimate for the effective LAI is marked in Figure 5 (top) with symbol '△'. In the case of low LAI, the ML estimate for $\mathrm{LAI_{eff}}$ is 0.66. Thus, the ML estimate is relatively close to the true value (0.42), even slightly more accurate than the Bayesian posterior mean estimate. We note that in this example case, the true spectra of ω_L and ρ_g were relatively close to the corresponding values assumed when computing the ML, and hence, the effect of uncertainties of this parameters in the $\mathrm{LAI_{eff}}$ estimates is minor.

The VI regression estimate is marked in Figure 5 (top) with symbol '▽'. In the low LAI case, the VI regression estimate equals to 1.70, and is thus clearly worse than the model-based estimates.

3.2.2. Example 2: high LAI case

In Example 2, $\mathrm{LAI_{eff}}$ was 4.87 and the stand was dominated by pine. The results of this example case are shown in the Figure 6. The Bayesian CM estimate equals to 4.56, and is thus rather close to the true value. In this case the posterior density of $\mathrm{LAI_{eff}}$ (Figure 6, top), is significantly wider than in Example 1 (Figure 5, top), implying that on high LAI stands, the estimate for $\mathrm{LAI_{eff}}$ has larger uncertainty. This stems from the saturation of the forest reflectance mentioned in Section 3.1: when the canopy gets very dense, the sensitivity of the reflectance measurements to a change in canopy LAI gets low. Note also that in both example cases, the posterior density of $\mathrm{LAI_{eff}}$ is skewed to the left; this is another indication of the higher uncertainty of the large LAI values caused by the saturation effect.

The posterior marginals for the leaf albedo ω_L and understory reflectance ρ_g in Example 2 are shown in the center and bottom of Figure 6, respectively. In this case, the posterior density of ω_L is very narrow, indicating a high credibility for the estimated ω_L. On the other hand, the posterior density of ρ_g is wide in Example 2, indicating high posterior uncertainty of ρ_g. These are again an intuitive results: While in the low LAI case, the sensitivity of reflectance measurements to ω_L is poor, leading to high posterior uncertainty of ω_L, in the high LAI case, the measured forest reflectance results nearly entirely from canopy scattering, with almost no understory contribution, leading to high credibility of the estimated ω_L and high uncertainty of ρ_g.

In Example 2, the ML estimate for $\mathrm{LAI_{eff}}$ ('△' in Figure 6, top) was 8.44, which is a heavily overestimated value. This error is again related to the saturation of the forest reflectance with high LAI. It is notable, that the ML estimate for $\mathrm{LAI_{eff}}$ is poor even though the the error in the variable ω_L behind the ML estimate is rather low (Figure 4). However, there is significant error in ρ_g and some error in β ($\beta = 0.71$ in the ML estimate vs. true value of 0.65).

In this example case, the VI regression estimate (represented by '▽' in Figure 6, top) was 4.07, i.e., slightly closer to the true value than in Example 1. This, however, does not mean that the VI regression estimates get generally better when LAI increases; in contrast, the set of simulations in the next section demonstrate that the overall accuracy of the VI regression estimates decreases with the increase of LAI.

3.2.3. Performance of the estimates over a set of 500 study stands

The performance of the Bayesian posterior mean estimates and the VI regression estimates is illustrated in Figure 7, showing a scatter plot of the estimated $\mathrm{LAI_{eff}}$ versus the true value of $\mathrm{LAI_{eff}}$ corresponding to each estimation method.

Generally, the Bayesian posterior mean estimates using the informative prior yield quite reliable estimates: In the entire range $[0, 5]$ of $\mathrm{LAI}_{\mathrm{eff}}$, these estimates possess only small/moderate errors, except for a few outliers (Figure 7, top left). Especially, in some dense pine dominated stands the $\mathrm{LAI}_{\mathrm{eff}}$ is largely overestimated, and in a few deciduous stands the $\mathrm{LAI}_{\mathrm{eff}}$ is underestimated. Overall, the error increases with increasing LAI – as expected, due to saturation effect discussed above.

The comparison of the scatter plots of the Bayesian estimates in Figure 7 (top left) and the ML estimates in Figure 3 shows that the Bayesian estimates are not as accurate as the ML estimates corresponding to models with correct parameters ω_L, ρ_g and β (Figure 3, left). However, the Bayesian estimates clearly outperform the ML estimates corresponding to parameters ω_L, ρ_g and β fixed to their population means (Figure 3, right). This observation is verified by the statistics of the estimates shown in Table 2: The RMSE of the Bayesian estimate is larger than the RMSE of the ML estimate with the correct parameters but significantly smaller than that of the ML estimate with the approximate parameters. The bias is, in fact, smaller than either of the ML estimates.

The results support the feasibility of the Bayesian approach to inversion of the reflectance model: Although the accuracy of the estimates decreases from the ideal case where the parameters are known, the Bayesian estimates tolerate the uncertainties of the reflectance model significantly better than ML estimates using approximate values for the parameters.

The scatter plot of the VI regression estimates is drawn in Figure 7 (top right). This plot shows significantly larger variation from the true $\mathrm{LAI}_{\mathrm{eff}}$ than the Bayesian CM estimates corresponding the informative prior, and in the small values of $\mathrm{LAI}_{\mathrm{eff}}$ (especially for $0 \leq \mathrm{LAI}_{\mathrm{eff}} \leq 1$), the VI regression estimates clearly feature a large positive bias. Table 2 reveals that the VI regression estimates are clearly less reliable than the Bayesian posterior mean estimates using the informative prior, but more accurate than the ML estimates using approximate parameters.

3.3. Effect of prior model and uncertainty quantification

The scatter plot of the Bayesian posterior mean estimate using the uniform prior is shown in Figure 7 (bottom). This plot and the statistics in Table 2 indicate that the accuracy of this estimate is in the same level as the accuracy of the VI regression estimate, i.e., the Bayesian estimates using the uniform prior are clearly more erroneous than those corresponding to the informative prior. Especially the overestimation of $\mathrm{LAI}_{\mathrm{eff}}$ in dense pine dominated stands and the underestimation of $\mathrm{LAI}_{\mathrm{eff}}$ in deciduous stands is significantly larger when uniform prior is used. This result suggests that the construction of the informative prior models for the parameters ω_L and ρ_g is advantageous over simply constraining these parameters.

Table 3 shows the RMSE% and the bias for the estimates of $\mathrm{LAI}_{\mathrm{eff}}$, ω_L, ρ_g and β based on Bayesian approach. The results are represented for both Bayesian estimates: those corresponding to uniform priors and those with the informative priors.

In cases of both prior models, the RMSEs of $\mathrm{LAI}_{\mathrm{eff}}$ and ω_L have little variation with respect to the majority species. For ρ_g the RMSE and bias of spruce-dominated stands are significantly better, which results from the fact that the expected true ρ_g of spruce-dominated stands is closest to the prior mean for ρ_g. The direction of the bias for the pine and deciduous stands points towards the prior mean. Another notable aspect is the relatively large overestimation of β on the spruce stands, which goes hand in hand with the overestimation of $\mathrm{LAI_{eff}}$ on spruce-dominated stands. The results of the table indicate that when using the informative prior, the estimation accuracy is generally fairly good. When using the uniform prior, the performance is consistently worse.

In addition to evaluating the point estimates, we also investigated the feasibility of the Bayesian estimates to quantify the (posterior) uncertainty of the model unknowns. For this purpose, we computed the coverage percentages of 95% credible intervals (CI%) for $\mathrm{LAI_{eff}}$, ω_L, ρ_g and β; this statistic is defined as the percentage of stands on which the true parameter value lies within the computed 95% credible interval (Equation (21)). The ideal value of the CI% would be 95%.

When using the informative priors, CI% of the effective LAI for the whole set of stands is 82.40%, which indicates a slight underestimation of the uncertainty of $\mathrm{LAI_{eff}}$. For the other parameters, the CI% is close to 95%, indicating that the approach gives a very good measure for the uncertainty of the estimated parameters. When using the uniform prior models for the parameters, CI%s are generally poorer. Especially, CI% of $\mathrm{LAI_{eff}}$ is only 59.20%, which indicates a large underestimation of the estimate uncertainty.

3.4. General discussion

In this study, cubic monotonic Hermite splines were used to enforce smoothness on the spectral variables ω_L and ρ_g and to implement dimension reduction. This representation has the strength that informative priors for the spectral variables can be constructed in a straightforward way, if expected value and variance of those variables is known at the node points. This is a clear advantage compared to some other possible low dimensional representations such as those based on principal components.

Overall, our results (Tables 2 and 3) support the use of informative prior models of the parameters ω_L and ρ_g in the Bayesian inference based on the reflectance model. The results show clearly the smallest estimation errors for $\mathrm{LAI_{eff}}$ when the informative prior models are used. Moreover, Bayesian approach with the informative prior models provides at least somewhat feasible means for quantifying the estimate uncertainties, yet the uncertainty of the $\mathrm{LAI_{eff}}$ was slightly underestimated in this numerical study. The informative prior formulation could be possibly further improved by including additional auxiliary information, for example seasonality, forest inventory data and spatial correlation.

4. Conclusions

Estimation of canopy LAI from hyperspectral imagery can be done via inversion of a forest reflectance model. Forest reflectance models, however, contain many other unknown, confounding variables in addition to LAI. In this paper, we investigated the effects of the model uncertainties on LAI estimates. Moreover, we studied whether the LAI estimates could be recovered from the errors caused by the model uncertainties by taking a Bayesian approach to forest reflectance model inversion. Moreover, we studied whether the Bayesian approach could be used of quantification of the estimate uncertainties.

The proposed approach was evaluated using realistic simulated data representing boreal forests. The performance of the Bayesian estimates was superior to the reference estimates in RMSE and bias. The results also show, that if parameters other than LAI are fixed to their best-guess value, the estimates based on inverting the reflectance model are often vastly erroneous. We also tested the effect of prior model formulation for the model unknowns; i.e., the informative prior formulation was compared with simple uniform prior formulation. With the informative priors the Bayesian estimates produced significantly smaller estimation errors and better estimates for the parameter uncertainty than with uniform priors.

The simulation results show that the Bayesian inference provides a feasible framework to account for uncertainties in secondary reflectance model variables. In contrast to empirical VI regression methods, the proposed approach can utilize the full information content of hyperspectral data and not only (pre)selected spectral bands. Additionally, the quantified estimate uncertainty is important in uncertainty quantification of climate models, if remotely sensed LAI is used as an input. In the future, the proposed approach has to be tested using real measurements to validate these promising simulation results.

Acknowledgements

This work was supported in part by the University of Eastern Finland (spearhead project Multiscale geospatial analysis of forest ecosystems and the doctoral school of the University of Eastern Finland) and in part by the Academy of Finland (Finnish Centre of Excellence of Inverse Problems Research 2012-2017, project number 250215, and projects 286390 and 135502).

[1] P. Gong, R. Pu, G. S. Biging, M. R. Larrieu, Estimation of forest leaf area index using vegetation indices derived from Hyperion hyperspectral data, IEEE Transactions on Geoscience and Remote Sensing 41 (6) (2003) 1355–1362. doi:10.1109/TGRS.2003.812910.

[2] J. Heiskanen, M. Rautiainen, P. Stenberg, M. Mõttus, V.-H. Vesanto, Sensitivity of narrowband vegetation indices to boreal forest LAI, reflectance seasonality and species composition, ISPRS Journal of Photogrammetry and Remote Sensing 78 (0) (2013) 1 – 14. doi:10.1016/j.isprsjprs.2013.01.001.

[3] F. Baret, G. Guyot, Potentials and limits of vegetation indices for LAI and APAR assessment, Remote sensing of environment 35 (2-3) (1991) 161–173. doi:10.1016/0034-4257(91)90009-U.

[4] G. Zheng, L. M. Moskal, Retrieving leaf area index (LAI) using remote sensing: Theories, methods and sensors, Sensors 9 (4) (2009) 2719–2745. doi:10.3390/s90402719.

[5] P. D'Odorico, A. Gonsamo, A. Damm, M. E. Schaepman, Experimental evaluation of Sentinel-2 spectral response functions for NDVI time-series continuity, IEEE Transactions on Geoscience and Remote Sensing 51 (3) (2013) 1336–1348. doi:10.1109/TGRS.2012.2235447.

[6] M. E. Schaepman, S. L. Ustin, A. J. Plaza, T. H. Painter, J. Verrelst, S. Liang, Earth system science related imaging spectroscopy – an assessment, Remote Sensing of Environment 113, Supplement 1 (0) (2009) S123 – S137. doi:10.1016/j.rse.2009.03.001.

[7] Y. Knyazikhin, M. A. Schull, P. Stenberg, M. Mttus, M. Rautiainen, Y. Yang, A. Marshak, P. Latorre Carmona, R. K. Kaufmann, P. Lewis, M. I. Disney, V. Vanderbilt, A. B. Davis, F. Baret, S. Jacquemoud, A. Lyapustin, R. B. Myneni, Hyperspectral remote sensing of foliar nitrogen content, Proceedings of the National Academy of Sciences 110 (3) (2013) E185E192. doi:10.1073/pnas.1210196109.

[8] F. Baret, S. Buis, Estimating canopy characteristics from remote sensing observations: Review of methods and associated prob-

lems, in: S. Liang (Ed.), Advances in Land Remote Sensing, Springer, 2008, pp. 173–201.

[9] K. M. Vanhatalo, M. Rautiainen, P. Stenberg, Monitoring the broadleaf fraction and canopy cover of boreal forests using spectral invariants, Journal of Quantitative Spectroscopy and Radiative Transfer 133 (2014) 482–488. doi:10.1016/j.jqsrt.2013.09.011.

[10] J. P. Kaipio, E. Somersalo, Statistical and Computational Inverse Problems, Springer, New York, 2005.

[11] Q. Zhang, X. Xiao, B. Braswell, E. Linder, F. Baret, B. Moore, Estimating light absorption by chlorophyll, leaf and canopy in a deciduous broadleaf forest using MODIS data and a radiative transfer model, Remote Sensing of Environment 99 (3) (2005) 357–371. doi:10.1016/j.rse.2005.09.009.

[12] M. Rautiainen, P. Stenberg, Application of photon recollision probability in coniferous canopy reflectance simulations, Remote Sensing of Environment 96 (2005) 98–107. doi:10.1016/j.rse.2005.02.009.

[13] T. Manninen, P. Stenberg, Simulation of the effect of snow covered forest floor on the total forest albedo, Agricultural and Forest Meteorology 149 (2009) 303–319. doi:10.1016/j.agrformet.2008.08.016.

[14] P. Stenberg, Simple analytical formula for calculating average photon recollision probability in vegetation canopies, Remote Sensing of Environment 109 (2007) 221–224. doi:10.1016/j.rse.2006.12.014.

[15] M. Mõttus, P. Stenberg, A simple parameterization of canopy reflectance using photon recollision probability, Remote Sensing of Environment 112 (2008) 1545–1551. doi:10.1016/j.rse.2007.08.002.

[16] P. Lukeš, P. Stenberg, M. Rautiainen, M. Mõttus, K. M. Vanhatalo, Optical properties of leaves and needles for boreal tree species in Europe, Remote Sensing Letters 4 (7) (2013) 667–676. doi:10.1080/2150704X.2013.782112.

[17] J. I. Peltoniemi, J. Suomalainen, E. Puttonen, J. Näränen, M. Rautiainen, Reflectance properties of selected arctic-boreal land cover types: field measurements and their application in remote sensing, Biogeosciences Discuss. 5 (2008) 1069–1095. doi:10.5194/bgd-5-1069-2008.

[18] M. Thérézien, S. Palmroth, R. Brady, R. Oren, Estimation of light interception properties of conifer shoots by an improved photographic method and a 3D model of shoot structure, Tree physiology 27 (10) (2007) 1375–1387. doi:10.1093/treephys/27.10.1375.

[19] W. Gilks, S. Richardson, D. Spiegelhalter (Eds.), Markov Chain Monte Carlo in Practice, Chapman & Hall, 1996.

[20] H. Haario, M. Laine, A. Mira, E. Saksman, DRAM: efficient adaptive MCMC, Statistics and Computing 16 (4) (2006) 339–354. doi:doi:10.1007/s11222-006-9438-0.

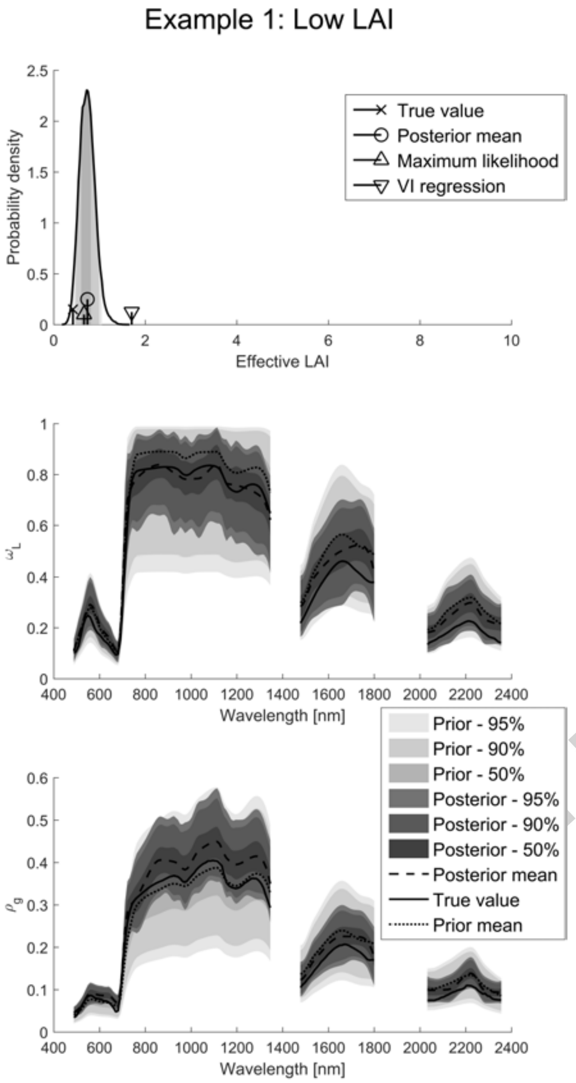

Figure 5: Posterior marginal densities of effective LAI (top), leaf albedo (center), and understory reflectance (bottom) for Example 1. The shaded areas in the top picture correspond to the 50%, 90% and 95% posterior CIs from dark to light grey, respectively.

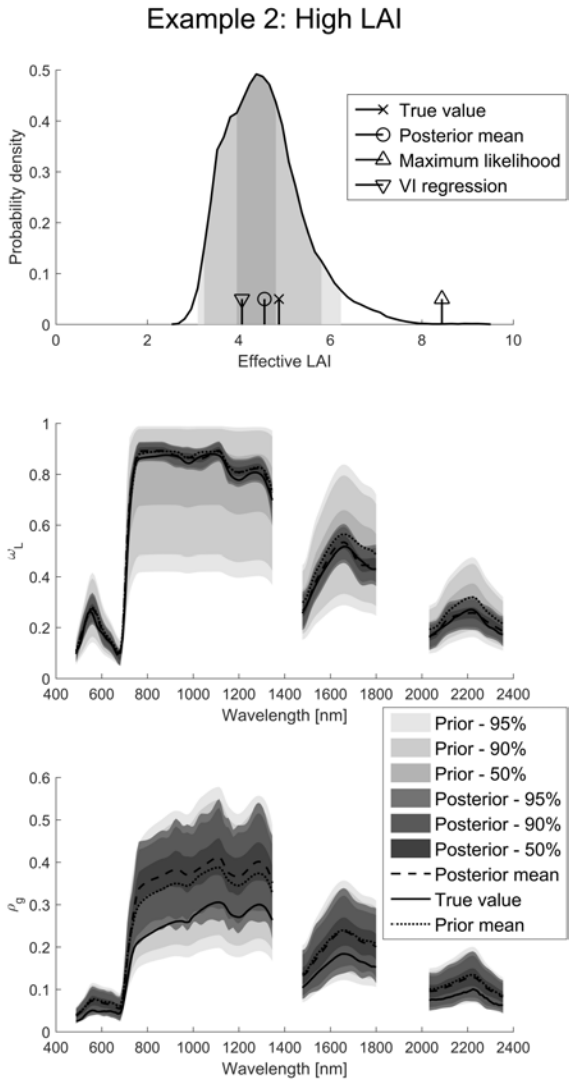

Figure 6: Posterior marginal densities of effective LAI (top), leaf albedo (center), and understory reflectance (bottom) for Example 2. The shaded areas in the top picture correspond to the 50%, 90% and 95% posterior CIs from dark to light grey, respectively.

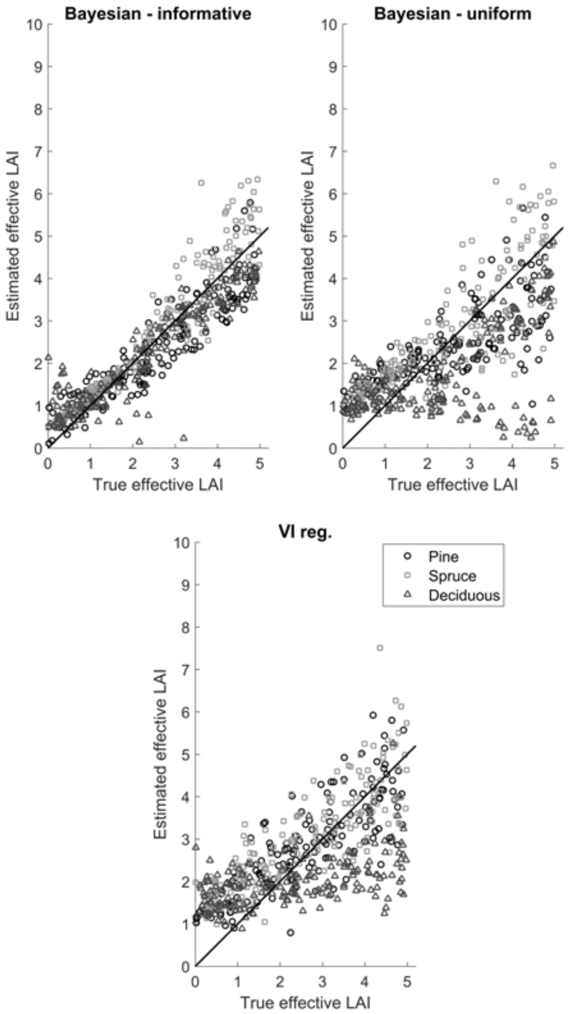

Figure 7: Estimated LAI_{eff} vs. true LAI_{eff} for the Bayesian posterior mean estimates (top left), empirical VI regression estimates (top right) and Bayesian posterior mean estimates using uniform prior (bottom), Pine dominated stands are marked with circles, spruce dominated with squares and deciduous with triangles.

Table 3: Relative RMSE and relative bias of Bayesian posterior mean estimates, and coverage percentage of 95% credible intervals, by the majority species. The spectral variables ω_L and ρ_g are divided to visible light (c. 480 – 700 nm), NIR (c. 750 – 1350 nm) and SWIR (c. 1500 – 2350 nm) components.

		Uniform prior			Informative prior		
		RMSE%	bias%	CI%	RMSE%	bias%	CI%
$\mathrm{LAI}_{\mathrm{eff}}$	pine	37.44	-5.44	63.29	23.44	-7.34	78.48
	spruce	36.02	12.24	69.51	23.51	12.44	86.59
	decid.	60.69	-27.43	46.07	26.83	-5.32	82.02
	all	45.88	-6.96	59.20	24.62	-0.0089	82.40
ω_L, vis.	pine	24.14	-2.09	99.64	12.06	2.88	99.19
	spruce	27.20	1.06	99.07	12.73	7.45	98.40
	decid.	30.95	7.03	99.01	11.25	-3.89	89.48
	all	28.29	2.23	99.23	12.17	1.65	95.48
ω_L, NIR	pine	14.31	-7.83	86.23	9.57	-4.17	90.60
	spruce	11.80	-5.25	94.84	4.42	-1.26	99.32
	decid.	17.92	-11.25	85.59	5.26	-1.61	97.16
	all	15.35	-8.34	88.83	6.70	-2.29	95.80
ω_L, SWIR	pine	21.36	-4.80	98.88	10.17	-0.15	99.82
	spruce	21.87	0.83	98.94	12.54	4.42	99.49
	decid.	23.41	-16.7	95.73	12.32	-8.35	88.16
	all	23.37	-9.11	97.78	12.39	-2.99	95.56
ρ_g, vis.	pine	48.94	30.57	99.37	30.98	-10.71	88.16
	spruce	66.06	54.57	99.91	13.93	2.59	72.00
	decid.	112.76	88.64	99.92	28.87	24.62	97.65
	all	72.45	53.93	99.74	26.59	2.97	93.77
ρ_g, NIR	pine	52.49	42.56	85.64	25.32	21.34	88.65
	spruce	34.58	22.13	93.69	10.03	3.28	98.88
	decid.	40.47	24.90	71.00	16.31	-6.31	92.76
	all	42.13	28.66	83.06	17.51	4.02	93.47
ρ_g, SWIR	pine	42.60	25.51	96.77	20.06	5.49	94.05
	spruce	46.03	32.02	98.68	17.01	13.74	99.52
	decid.	60.65	51.77	86.22	20.43	16.56	91.18
	all	51.08	36.94	93.64	19.41	11.85	94.82
β	pine	15.62	-0.16	89.24	13.06	-3.59	98.73
	spruce	20.68	7.34	87.80	22.43	12.96	91.46
	decid.	18.86	-12.36	84.27	6.35	1.74	97.19
	all	18.87	-3.63	87.00	13.24	3.20	95.80